A Novel High-Efficient and Miniaturized Operating Method for Ultra-Fast Vacuum Switch

Weijie Wen, Hezhi Jin, Jiawei He, Bin Li, Changhong Zhang, Wei Chen, Qingyao Sun, and Jinghan Fan

***Abstract*—As one of the most important component in mechanical and hybrid dc breaker (MCB and HCB), operating time of ultrafast vacuum switch (VS) determines the breaking speed of MCB and HCB. However, limited by the high capacitive storage energy requirement of Thomason-coil actuator (TCA), the low-efficiency and large-volume of operating mechanism are main restrictions for wide application of ultrafast VS. This article proposes a high-efficient and miniaturized operating method for ultrafast VS by recycling the residual energy in capacitor banks for sequential open- and close-operations (O-C). Mathematical model of ultrafast VS during the sequential O-C operation process is established, and the prototype with rated parameters of 3.6 kV/2.5 kA/1ms is developed for experimental verification. The research shows that by using the proposed method, the total required capacitive storage capacity for sequential O-C operation is decreased by 50%, from 2038 to 1019 J, resulting in the doubled operating efficiency. In addition, the cost and volume of the operating mechanism for ultrafast VS are decreased significantly.**

***Index Terms*—DC breaker, high-efficient, Thomason-coil actuator, ultrafast vacuum switch.**

I. Introduction

With demand for fast fault current interruption and flexible load current interruption in dc system, dc circuit breakers (DCB) are the key equipment for dc networking. Up to now, instead of the solid state dc breaker (SSCB), the mechanical and hybrid DCB (MCB and HCB) have been successfully used in practical demonstration projects [1], [2]. The reason is MCB and HCB have ultrafast vacuum switch (VS) for long-term load current conduction, generating advantages of low-operating losses and no need for complex cooling system [3], [4]. According to the working principle of MCB and HCB, the operating time of ultrafast VS determines when the transient interruption voltage (TIV) can be established [5], [6], meaning operating time of ultrafast VS determines the breaking-speed of DCB [7], [8], [9].

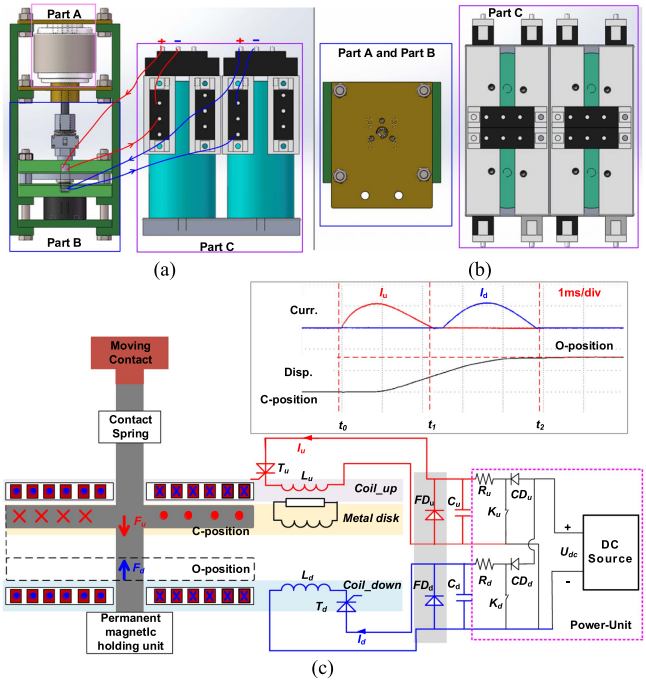

Fig. 1. Basic structure of ultrafast VS. (a) Front-view of ultrafast VS. (b) Top-view of ultrafast VS. (c) Existing drive circuits for ultrafast VS and its operating characteristics.

As shown in Fig. 1(a) and (b), an ultrafast VS consists of three parts as follows [10], [11]. 1) Part-A is the vacuum interrupter which has static contact and moving contact inside. Part-B and Part-C form the operating mechanism. 2) Part-B is the mechanical part, and it is mainly composed of Thomason-coil actuator (TCA) [12], [13] and permanent magnetic holding unit (PM-HU). 3) Part-C is the energy storage unit, and it is mainly composed of precharged capacitor banks and thyristor modules, whose function is to supply energy for TCA to complete open- and close- (O- and C-) operations of ultrafast VS.

The typical drive circuit for ultrafast VS and its operating characteristics are illustrated in Fig. 1(c). Taking the O-operation process as example, the basic working principle is: by triggering T_u and T_d in sequence, C_u and C_d discharges through coil_up

Manuscript received 13 November 2023; revised 23 January 2024 and 28 March 2024; accepted 20 April 2024. Date of publication 23 May 2024; date of current version 20 June 2024. This work was supported in part by the National Key Research and Development Program of China under Grant 2022YFB2403601, in part by the National Natural Science Foundation of China under Grant 52277120, and in part by the Basic and Applied Basic Research Foundation of Guangdong Province under Grant 2022A1515240068. Recommended for publication by Associate Editor X. Pei. *(Corresponding authors: Jiawei He; Bin Li.)*

Weijie Wen, Hezhi Jin, Jiawei He, Bin Li, Qingyao Sun, and Jinghan Fan are with the Key Laboratory of Smart Grid of Ministry of Education and National Industry-Education Platform for Energy Storage, Tianjin University, Tianjin 300072, China (e-mail: weijie.wen@tju.edu.cn; hejiawei1991@tju.edu.cn; binli@tju.edu.cn).

Changhong Zhang and Wei Chen are with the Maintenance & Test Center of EHV Power Transmission Company, China Southern Power Grid, Guangzhou 510663, China.

Color versions of one or more figures in this article are available at https://doi.org/10.1109/TPEL.2024.3396211.

Digital Object Identifier 10.1109/TPEL.2024.3396211

(L_u) and coil_down (L_d), respectively, in sequence, generating eddy current and electromagnetic force (F_u and F_d) in the metal disk with different directions. F_u can accelerate the moving contact first and then, F_d decelerate it to avoid strong mechanical shock, ensuring the moving contact can move from close-position (C-position) to open-position (O-position) smoothly [14], [15], [16]. The C-operation process is just opposite with the O-operation process.

Just as shown in Fig. 1(c), up to now, depending on if freewheel diodes exist or not, there are two kinds of drive circuit as follows [17], [18]. 1) The first is the case without (FD_u and FD_d) parallel with relative capacitors (C_u and C_d) [10]. In this case, because the oscillation between C_u and L_u (C_d and L_d) is underdamping, T_u and T_d are extinguished at current zero point, and part of the energy returns to (C_u and C_d), resulting in residual energy in the form of reversal electric field energy in (C_u and C_d). When dc source recharges (C_u and C_d) to the preset voltage in preparation for the next operation, the residual energy is dissipated by the charging resistors (R_u and R_d), meaning the residual energy is wasted, and the precharged energy in (C_u and C_d) are totally consumed for this O-operation. 2) The second is the case with (FD_u and FD_d) parallel with relative capacitors (C_u and C_d) [18]. In this case, after voltage on C_u (C_d) decreases to zero, the current through L_u (L_d) flows through FD_u (FD_d), meaning the precharged energy is totally dissipated in coils (L_u and L_d) gradually without returning back to the capacitor banks. Therefore, for the existing two drive circuits for ultrafast VS, no matter (FD_u and FD_d) exist or not, all the precharged energy in capacitor banks is dissipated during one operation process.

According to the previous research data [10], with moving part of 5 kg, moving over 13 mm within 2.3 ms needs two capacitor banks of 2.5 mF with precharged voltage of 1.3 kV (4.225 kJ). Because the operating-time is the most important performance indicator and speed of moving part is variable during the operation process, average speed of moving part is used to represent the transformed kinetic energy. Therefore, only $78\text{J} = 5\,\text{kg}\times(13/2.3\,\text{m/s})^2$ is transferred to be the kinetic energy, and the operating efficiency is only 1.89%. In other words, the low-operating efficiency of existing drive circuits requires high capacitive energy capacity in ultrafast VS.

With only two capacitor banks for O-operation illustrated, the front- and top-view of ultrafast VS with same scale of the developed prototype (detail3.6 kV/2.5 kA/1ms) in this article is shown in Fig. 1(a) and (b). Parameters of capacitor banks in Part-C is $2\times2\times520\,\mu$F with rated voltage of 1.2 kV. It should be noted, with the equivalent inductance and resistance of the coil very small, the discharge of the capacitor is similar to a short-circuit discharge. In this case, electric charge in the capacitors is released instantaneously, resulting in a pulse discharging current with amplitude of 2∼3 kA, which may cause serious heating in electrolytic capacitors, while film capacitors are able to withstand the pulse current with high-amplitude. In addition, the lifetime of electrolytic capacitors is much shorter than film capacitors. Therefore, from the perspective of reliability, metal film capacitors instead of electrolytic capacitors are widely used in operating mechanism of ultrafast vacuum switch. Besides, to prevent the voltage drop of metal film capacitors due to self-leaking, the precharged circuits maintain the charging to the capacitors before the fault occurs. Once the fault occurs, the precharged circuits are disconnected and the precharged capacitors discharge to the coil, enabling successful sequential O-C operations.

However, limited by the low energy density, dimensions of the used commercial metal film capacitor banks are $2\times2\times\Phi85$ mm$\times$175 mm. Without considering thyristor modules, volume of Part-C ($2\times2\times\Phi85$ mm$\times$175 mm) is much larger than the other two parts (140 mm$\times$120 mm$\times$260 mm), meaning Part-C is the largest part in ultrafast VS. In addition, sequential C-operation within ∼200 ms after O-operation is required for ultrafast VS in DCB, and the existing scheme is to configure another two capacitor banks, meaning volume and cost of Part-C is further doubled. Therefore, the low energy density of commercial metal film capacitors results in large-volume of Part-C, and the requirement of sequential C-operation could further lead to doubled volume and cost of Part-C in ultrafast VS.

The rest of this article is organized as follows. To tackle these problems, a high-efficient and miniaturized operating method for ultrafast VS is proposed in this article. The basic working principle is recycling the residual energy after the first O-operation for the sequential C-operation in ultrafast VS, which is presented in Section II. Simulation model is established in Section III for prototype design. Then, prototype development and experimental verification are carried out in Section IV. Finally, Section V concludes this article.

II. Proposed High-Efficient Operating Method Based on Energy Recycling

For the sake of reclosing to permanent fault, operating mechanism of ac breakers should be capable of open-close-open operations (O-C-O) so that the fault current could be successfully interrupted twice. However, adaptive reclosing strategies for DCB have proposed in [19] and [20], meaning permanent and transient fault can be distinguished in advance before the reclosing, only sequential open-close operations (O-C) is required for ultrafast VS in DCB. Moreover, only fast O-operation (2–3 ms) is needed, and the C-operation could be relatively slow.

As shown in Fig. 2(a), to enable the sequential O-C operation of ultrafast VS, four capacitor banks are configured in the conventional drive circuit in Part-C of an ultrafast VS. As shown in Fig. 2(c), with $T_{u\text{-}o}$, $T_{d\text{-}o}$ triggered in sequence, $C_{u\text{-}o}$, $C_{d\text{-}o}$ discharges through L_u and L_d, respectively, generating acceleration force ($F_{u\text{-}o}$) and deceleration force ($F_{d\text{-}o}$) applied on metal disk to complete the smooth O-operation; then, after ∼200 ms for the deionization of fault point, with $T_{d\text{-}c}$, $T_{u\text{-}c}$ triggered in sequence, $C_{d\text{-}c}$, $C_{u\text{-}c}$ discharges through L_d and L_u respectively, generating acceleration force ($F_{d\text{-}c}$) and deceleration force ($F_{u\text{-}c}$) applied on metal disk to complete the smooth C-operation. As mentioned before, for the conventional drive circuit with or without freewheel didoes parallel with relative capacitor banks, the precharged energy in these four capacitor banks is totally consumed for the sequential O-C operations, resulting in quite low operating efficiency.

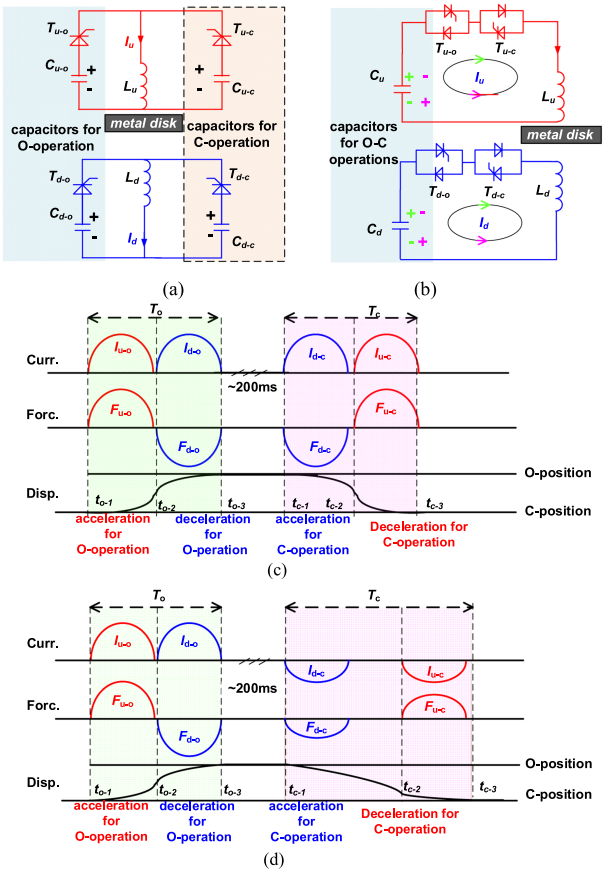

Fig. 2. Drive circuit to enable sequential O-C operations of ultrafast VS. (a) Conventional drive circuit. (b) Proposed drive circuit. (c) Operating characteristics of VS with conventional drive circuit. (d) Operating characteristics of VS with proposed drive circuit.

Aimed to increase operating efficiency, the novel drive circuit shown in Fig. 2(b) is proposed. It can be seen, only two capacitor banks are configured for sequential O-C operation. Referring to the operating characteristics in Fig. 2(d), with $T_{\text{u-o}}$, $T_{\text{d-o}}$ triggered in sequence, C_{u}, C_{d} with positive precharged voltage discharges through L_{u} and L_{d} respectively, generating acceleration force ($F_{\text{u-o}}$) and deceleration force ($F_{\text{d-o}}$) to complete the smooth O-operation. Along with residual energy returning back to C_{u} and C_{d}, negative voltage appears on (C_{u} and C_{d}) whose amplitude is 40%–50% of the initial positive voltage. Then, after ~200 ms for the deionization of fault point, with $T_{\text{d-c}}$, $T_{\text{u-c}}$ triggered in sequence, C_{d}, C_{u} with negative voltage discharges through L_{d} and L_{u} again, generating pulse current with anticlockwise direction in Fig. 2(b) (indicated by the pink arrow). The induced electromagnetic force ($F_{\text{d-c}}$ and $F_{\text{u-c}}$) is always tending to push the metal disk away from (L_{d} and L_{u}), and force direction is not relevant with the detailed direction of pulse current, meaning $F_{\text{d-c}}$ and $F_{\text{u-c}}$ is still the acceleration and deceleration force for metal disk to complete smooth C-operation.

It should be noted, because amplitudes of the negative voltage on capacitor banks for C-operation are lower than the positive voltage for O-operation, the pulse current and electromagnetic force in C-operation are also smaller than O-operation, meaning the metal disk takes more time to move over the full stroke during the C-operation process [$T_{\text{c}} > T_{\text{o}}$ in Fig. 2(d)], and C-operation is slower than O-operation. As mentioned before, there is no need for fast C-operation of VS in DCB, and using the proposed drive circuit for VS in DCB would not sacrifice both fast breaking and reclosing performance of DCB.

Comparing Fig. 2(a) and (b), in the proposed driving circuit, by using two thyristor antiparallel with diode which enables the active turning-ON ability of bidirectional current, the residual energy in capacitor banks after O-operation could be recycled for the sequential C-operation, and the two capacitor banks in Fig. 2(a) specially configured for C-operation ($C_{\text{u-c}}$ and $C_{\text{d-c}}$) are completely saved. Therefore, compared with the conventional drive circuit, only 50% of the precharged energy is required for sequential O-C operation of ultrafast VS by using the proposed drive circuit, meaning a significant improvement of operating efficiency.

III. Simulation of Ultrafast VS Based on the Proposed Operating Method and Prototype Design

A. Simplified Mathematical Model of Ultrafast VS During Sequential O-C Operation

The method using TCA for both acceleration and deceleration of metal disk is first proposed in [10], where the metal disk is equivalent by m parallel loop-circuits with inductor and resistor in series (LR circuit). The larger m is, the more accurate the simulation is, and the nonuniform distribution of eddy current inside the metal disk can also be taken into consideration. However, for the case when frequency of pulse current in metal disk is less than 1 kHz, the uneven distribution of eddy current has slight impact on the simulation results, meaning by setting $m = 1$, the simplified simulation model can ensure both high-accuracy and fast simulation speed. Therefore, the metal disk is equivalent by only one LR loop-circuit in this part.

From the prospective of equivalent electrical circuits, TCA consists of three mutually coupled loop-circuits as follows: 1) The first is up-coil-circuit with C_{u} and L_{u} in series; 2) the second is metal-disk-circuit composed of passive LR circuit; and 3) the third is the down-coil-circuit with C_{d} and L_{d} in series. The metal-disk-circuit could move to any position between O-position and C-position; the up-coil-circuit and down-coil-circuit are static during the whole process.

Referring to Fig. 2(d), depending on if there are currents in the three loop-circuits, the whole O-C operation process could be divided into five stages as follows: 1) $t_{\text{o-1}} \sim t_{\text{o-2}}$; 2) $t_{\text{o-2}} \sim t_{\text{o-3}}$; 3) $t_{\text{o-3}} \sim t_{\text{c-1}}$; 4) $t_{\text{c-1}} \sim t_{\text{c-2}}$; and 5) $t_{\text{c-2}} \sim t_{\text{c-3}}$.

For the first stage: $t_{\text{o-1}} \sim t_{\text{o-2}}$ (the acceleration period of metal disk in O-operation), with C_{u} discharging through the up-coil-circuit, currents with initial values of zero flow in up-coil-circuit (I_{u}) and metal-disk-circuit (I_{md}), and the state equation is shown in (1), where Ψ_{u} and Ψ_{md} are the flux linkage of up-coil-circuit and metal-disk-circuit. U_{Cu} is the voltage on C_{u}, and its initial value is the precharged voltage on C_{u}. R_{u} and R_{md} is the equivalent resistance of up-coil-circuit and metal-disk-circuit. $F_{\text{u-o}}$ is the induced electromagnetic force between up-coil-circuit and metal-disk-circuit which will accelerate the metal disk to move

away from the up coil. z is the displacement of metal disk away from up-coil-circuit. f_{VI} is the output force of vacuum interrupter which is given in relative datasheet, f_{holding} is the output force of PM_HU. m_{load} is the total mass of all the moving parts.

$$\begin{cases} \frac{d\psi_{\mathrm{u}}}{dt} = U_{Cu} - R_u I_u \\ \frac{d\psi_{md}}{dt} = 0 - R_{md} I_{md} \\ \frac{dU_{Cu}}{dt} = -\frac{C_u}{I_u} \\ \frac{d^2 z}{dt^2} = \frac{(F_{u-o} - f_{holding} - f_{VI})}{m_{load}} \end{cases}. \tag{1}$$

Because Ψ_{u} and Ψ_{md} are field quantities, which can be expressed by inductance and current, (2) is deduced for simplicity, where L_{u} and L_{md} is the equivalent inductance of up-coil-circuit and metal-disk-circuit, and $M_{\mathrm{u,md}}$ is the mutual inductance between them. It should be noted, with metal disk moving, L_{u} and L_{md} are constant with z, and only $M_{\mathrm{u,md}}$ changes with z.

$$\begin{aligned} \frac{d\psi_{\mathrm{u}}}{dt} &= L_u \cdot \frac{dI_u}{dt} + M_{u,md} \cdot \frac{dI_{md}}{dt} + I_{md} \cdot \frac{\partial M_{u,md}}{\partial z} \cdot \frac{dz}{dt} \\ \frac{d\psi_{md}}{dt} &= M_{u,md} \cdot \frac{dI_u}{dt} + L_{md} \cdot \frac{dI_{md}}{dt} + I_u \cdot \frac{\partial M_{u,md}}{\partial z} \cdot \frac{dz}{dt} \\ F_{u-o} &= \frac{dM_{u,md}}{dz} \cdot I_u \cdot I_{md} \end{aligned} \tag{2}$$

For the second stage: $t_{\mathrm{o\text{-}2}} \sim t_{\mathrm{o\text{-}3}}$ (the deceleration period of metal disk in O-operation), currents flow in down-coil-circuit (I_{d}) and metal-disk-circuit (I_{md}). The state equation is shown in (3), where the expression of Ψ_{d}, Ψ_{md} and $F_{\mathrm{d\text{-}o}}$ is shown in (4).

It should be noted, the initial value of I_{d} is zero and the initial value of I_{md} is the terminal value of the first stage. Ψ_{d} is the flux linkage of down-coil-circuit. U_{Cd} is the voltage on C_{d}, and its initial value is the precharged voltage on C_{d}. R_{u} is the equivalent resistance of down-coil-circuit. $F_{\mathrm{d\text{-}o}}$ is the induced electromagnetic force between down-coil-circuit and metal-disk-circuit which can decelerate the metal disk to prevent its strong mechanical shock to the down-coil, and ensure the soft landing.

$$\begin{cases} \frac{d\psi_d}{dt} = U_{Cd} - R_d I_d \\ \frac{d\psi_{md}}{dt} = 0 - R_{md} I_{md} \\ \frac{dU_{Cd}}{dt} = -\frac{C_d}{I_d} \\ \frac{d^2 z}{dt^2} = \frac{(F_{d-o} - f_{holding} - f_{VI})}{m_{load}} \end{cases} \tag{3}$$

$$\begin{aligned} \frac{d\psi_{\mathrm{d}}}{dt} &= L_d \cdot \frac{dI_d}{dt} + M_{d,md} \cdot \frac{dI_{md}}{dt} + I_{md} \cdot \frac{\partial M_{d,md}}{\partial z} \cdot \frac{dz}{dt} \\ \frac{d\psi_{md}}{dt} &= M_{d,md} \cdot \frac{dI_d}{dt} + L_{md} \cdot \frac{dI_{md}}{dt} + I_d \cdot \frac{\partial M_{d,md}}{\partial z} \cdot \frac{dz}{dt} \\ F_{d-o} &= \frac{dM_{d,md}}{dz} \cdot I_d \cdot I_{md} \end{aligned}. \tag{4}$$

For the third stage: $t_{\mathrm{o\text{-}3}} \sim t_{\mathrm{c\text{-}1}}$ (the period of metal disk keeping static at the O-position), current only flows in metal-disk-circuit (I_{md}), and it decays with time according to the zero-input response of LR circuit. The state of equation is expressed in

$$\begin{cases} \frac{d\psi_{md}}{dt} = 0 - R_{md} I_{md} \\ \frac{d\psi_{md}}{dt} = L_{md} \cdot \frac{dI_{md}}{dt} \end{cases}. \tag{5}$$

For the fourth stage: $t_{\mathrm{c\text{-}1}} \sim t_{\mathrm{c\text{-}2}}$ (the acceleration period of metal disk in C-operation), with the negative voltage on C_{d} discharging back in down-coil-circuit, currents flow in down-coil-circuit and metal-disk-circuit again, and the state equation is the same with the second stage [(3) and (4)], but the initial values of state variable (U_{cd}) is different from the second stage.

For the fifth stage: $t_{\mathrm{c\text{-}2}} \sim t_{\mathrm{c\text{-}3}}$ (the deceleration period of metal disk in C-operation), with negative voltage on C_{u} discharging back in up-coil-circuit, the state equation is the same with the first stage [(1) and (2)], and also the initial values of state variables are different from the first stage.

With inductances and mutual inductances (L_{u}, L_{md}, L_{d}, $M_{\mathrm{u,md}}$, $M_{\mathrm{d,md}}$) extracted by solving static magnetic field based on finite element method in advance, if f_{holding} is also known, the differential equations in the five stages can be easily solved by Runge-Kutta method. Therefore, how to obtain f_{holding} is discussed in Section III-B.

B. Output Characteristic of PM-HU and Its Design

For VS in open-state, a negative holding force is needed to overcome the contact closing force, keeping the moving contact at the O-position away from the static contact. For VS in close-state, a positive holding force is needed to overcome the contact counterforce, keeping the static and moving contacts are closely compressed to obtain ultralow conduction resistance in the order of $\mu\Omega$. Therefore, bistable holding unit which could provide bidirectional holding force is essential for VS.

Holding force should be designed according to the surge current that might flow through contacts in vacuum interrupter [10]. Considering surge current through VS in DCB usually does not exceed 20 kA, the recommended holding force is 0.8–1kN, given in datasheet of commercial vacuum interrupters [21].

Compared with the bi-stable spring unit used in high-voltage VS with long-stroke [10], PM-HU based on permanent magnet is more suitable for low-voltage VS with short-stroke. The reason is with full-stroke (∼5 mm) in low-voltage VS much smaller than high-voltage VS (20–30 mm), PM-HU has advantages of simple-structure, light-moving part, easy-installment, and low-inertia than bistable spring unit.

Detailed diagram of PM-HU proposed by us is illustrated in Fig. 3(a), and it consists four components that are the connecting rod (7075 aviation aluminum-alloy), the static core and the moving core (pure iron DT4), and the permanent NdFeB magnet (N48SH). Because the magneto-conductivity of the connecting rod is almost equal to air, it has no effects on the magnetic field distribution.

The holding force between the static and moving core (pure iron DT4) can be expressed by (6) where $\vec{B}$ and $\vec{H}$ is the magnetic induction strength and magnetic field strength of air gap near the surface of moving core; μ_0 is the permeability of air-gap between moving and static core; and S is the intersection area between moving and static core.

$$f_{holding} = \int \frac{\vec{B} \cdot \vec{H}}{\mu_0} \cdot dS \tag{6}$$

To obtain f_{holding}, static magnetic field model of PM-HU is established in Ansoft Maxwell based on finite element method. In the simulation, key parameters for permanent NdFeB magnet

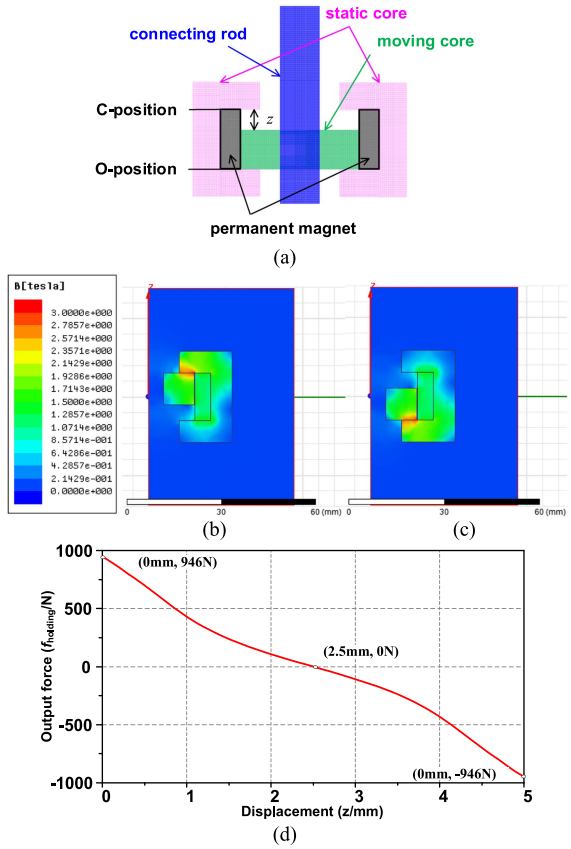

Fig. 3. Structure and output characteristics of PM-HU. (a) Diagram of PM-HU. (b) Magnetic field distribution of PM-HU at C-position. (c) Magnetic field distribution of PM-HU at O-position. (d) Output characteristics of PM-HU.

are H_c (1000 kA/m) and B_r (1.38T), which can be found in the datasheet of NdFeB [22]. Key characteristic of static and moving core (pure iron DT4) is the magnetization curve (*B-H* curve) which is given in datasheet of this material. The simulated magnetic field distribution with moving core at C-position and O-position is illustrated in Fig. 3(b) and (c), and they are completely symmetrical.

By changing z from 0 to 5 mm with the step of 0.1 mm, the output characteristic of PM-HU is obtained, just as shown in Fig. 3(d). By indexing $f_{\text{holding}}(z)$ according to the displacement of metal disk (z), mathematical model shown by (1)–(5) could be solved successfully.

Physical dimensions of the static and moving core are determined by sensitivity analysis to obtain the desired holding force, and to ensure the mass of moving core is as small as possible. The physical dimensions of moving core are listed as follows: inner radius is 5 mm; outer radius is 30 mm; and height is 10 mm. With mass density of 7.8759 g/mm^3, mass of moving core is only 50 g, far less than the bistable spring unit (200 g) in [10] for high-voltage VS with long-stroke, and this is absolutely beneficial for the high-efficient and fast operating of VS.

C. Prototype Design and the Simulation Results

In this part, an ultrafast VS prototype with rated parameters of 3.6 kV/2.5 kA/1ms is developed for experimental verification.

TABLE I
VS PROTOTYPE DESIGN OF 3.6KV/2.5KA/1MS

Parameter	Value	Parameter	Value
C (mF)	1.040	h_p (mm)	8
U_0 (V)	900	R_a (mm)	0
h_c (mm)	6	R_b (mm)	50
R_1 (mm)	12.5	m_{load} (kg)	1
R_2 (mm)	50	s (mm)	3
n	48	z_1 (mm)	5
ρ_1 ($\Omega\cdot$m)	1.75*10^{-8}	ρ_2 ($\Omega\cdot$m)	2.83*10^{-8}

A total of 3.6 kV is the rated voltage; 2.5 kA is the rated current; and 1ms is the rated O-operation time, which is actually the time when the contacts separation of vacuum interrupter is large enough to withstand TIV of 1.5 p.u. Based on the mathematical model in Section III-A, structural and electrical parameters of the prototype are designed by using the optimization method proposed by us in [10], and they are listed in Table I. Where C is the capacitance of capacitors (C_u, C_d, DKMJ1.2-520 provided by NINGBO HARONG ELECTRIC); U_0 is the initial precharged voltage of C_u and C_d; h_c, R_1 and R_2 are the height, the inner radius and the outer radius of the coil respectively; n is the number of turns of the coil (made by copper wire); h_p, R_a and R_b are the height, the inner radius and the outer radius of the metal disk (made by 7075 aviation aluminum-alloy), respectively; m_{load} is the mass of moving parts; s is the initial distance between metal disk and coil; z_1 is the full-stroke of ultrafast VS; ρ_1 and ρ_2 are the resistivity of copper and 7075 aviation aluminum-alloy, respectively.

Based on the structural parameters of coils and metal disk in Table I, inductances (L_u, L_{md}, L_d, $M_{u,md}$, $M_{u,md}$) are extracted by finite element method. With f_{holding} known in Section III-B, the mathematical model in the form of differential equations in Section III-A is solved, and the results are illustrated in Fig. 4 .

The simulated operating characteristics of the sequential O-C operation are consistent with the theoretical analysis in Fig. 2(d). As for the O-operation process, during the acceleration period of O-operation (0–1 ms), C_u discharges through L_u, generating pulse current ($I_{u\text{-}o}$) with amplitude of 2.4 kA and the acceleration force ($F_{u\text{-}o}$) with amplitude of 13.6 kN. After this discharge of C_u, voltage on C_u (U_{Cu}) changes from 900 to -373 V, meaning $\sim$17% of the initial energy returns back to C_u. Then, during the deceleration period of O-operation (1–2 ms), C_d discharges through L_d, resulting in voltage on C_d (U_{Cd}) changes from 900 to -408 V. The metal disk moves over 5 mm from C-position to O-position within 2 ms.

After the O-operation, 200 ms is usually reserved for the deionization of fault point. During this period (2–202 ms), the metal disk is kept static at the O-position by PM-HU and the eddy current in metal-disk-circuit decays to zero gradually according to LR circuit with zero-input response, just as shown in Fig. 4(e).

As for the C-operation process, C_d and C_u with residual voltage of -408 and -373 V discharges reversely through L_d and L_u, respectively, generating the pulse current ($I_{d\text{-}c}$ and $I_{u\text{-}c}$) in Fig. 4(c) and electromagnetic force ($F_{d\text{-}c}$ and $F_{u\text{-}c}$) in Fig. 4(d), whose amplitudes are smaller than the O-operation.

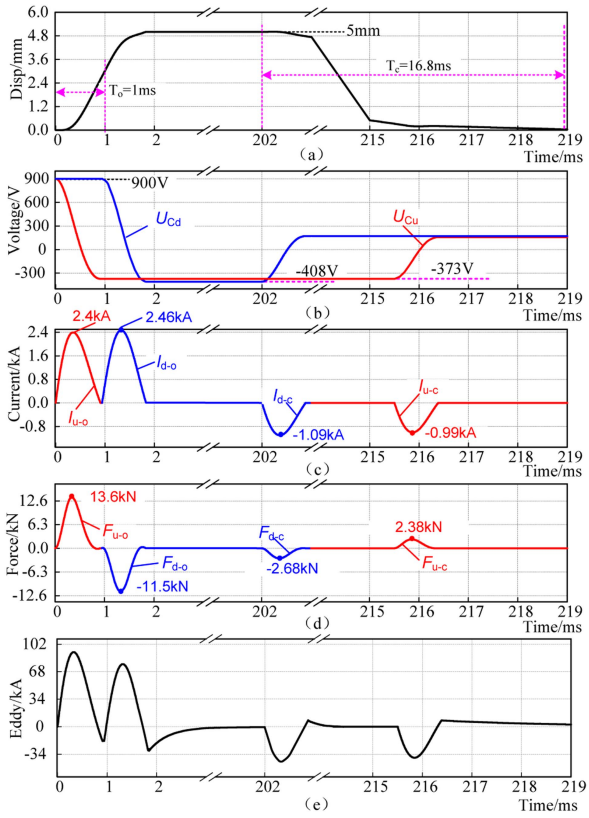

Fig. 4. Simulated operating characteristics of the prototype. (a) Displacement of the metal disk. (b) Voltage on capacitors (C_u, C_d). (c) Current in coil L_u and L_d. (d) Induced electromagnetic force of the metal disk. (e) Eddy current in metal disk.

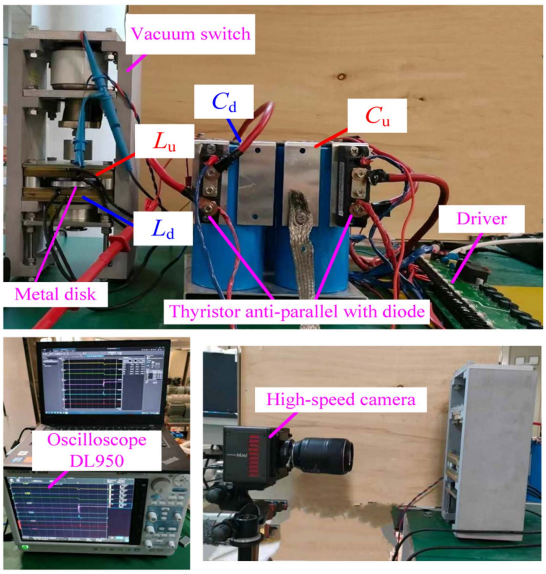

Fig. 5. Experimental platform.

The metal disk moves over 5 mm from O-position to C-position within 17 ms.

It should be noted the opening-time of VS indicates the time for contact separation increasing from 0 to the distance which is enough to withstand TIV. Because the breakdown field strength

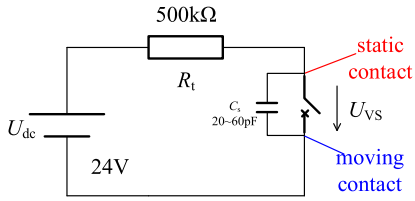

Fig. 6. Test circuit to obtain the accurate time of contacts separation and contacts closing.

of vacuum gap is ∼30 kV/mm [23], half of the stroke (2.5 mm) is set to withstand the TIV by taking a safety margin into consideration. The other half of the stroke is reserved for the deceleration of moving part. The closing-time indicates the time interval for contact separation changing from the full-stroke to zero. Therefore, according to Fig. 4(a), the opening-time of VS is 1 ms, and the closing-time of VS is 17 ms.

IV. Experiments Verification

A. Experimental Platform

According to the proposed drive circuit shown in Fig. 2(b) and the parameters listed in Table I, a prototype of ultrafast VS (3.6 kV/2500 A/1ms) has been successfully developed, and the picture is illustrated in Fig. 5.

In the tests, currents were measured by two Rogowski coils (CWT140B/4/1000 provided by PEM); voltages were measured by two high voltage differential probes (S19010A provided by Sapphire); and all the signals were recorded by oscilloscope (DL950 provided by Yokogawa). The movement of metal disk is recorded by high-speed camera (FASTCAM Mini provided by Photron) which can capture the position of metal disk with a time step of 100μs. The thyristors antiparallel with diode were MFX110A provided by SHANGZHENG.

Except for the drive circuits for ultrafast VS shown in Fig. 2(b), a test circuit to obtain the accurate time of contacts separation and contacts closing is designed, as shown in Fig. 6. In the test circuit, a dc voltage source (24 V) in series with a resistor (500 kΩ) is connected by the static and moving contacts inside the vacuum interrupter.

When ultrafast VS is closed, static contact and moving contact are compressed together, and the equivalent resistance is in the order of $\mu\Omega$, resulting in the voltage across the contacts (U_{VS}) is zero. During the O-operation process, when contacts are separated, U_{VS} increases to 24 V gradually, which is caused by the charging effect of parasitic capacitor across contacts (C_s) by U_{dc} through R_t. Therefore, the moment when U_{VS} starts to increase from zero indicates the moment when contacts are separated. When ultrafast VS is open, static contact and moving contact are separated, resulting in U_{VS} is equal to 24 V. During the C-operating process, the moment when U_{VS} starts to decrease from 24 V indicates the moment when static contact and moving contact get in touch.

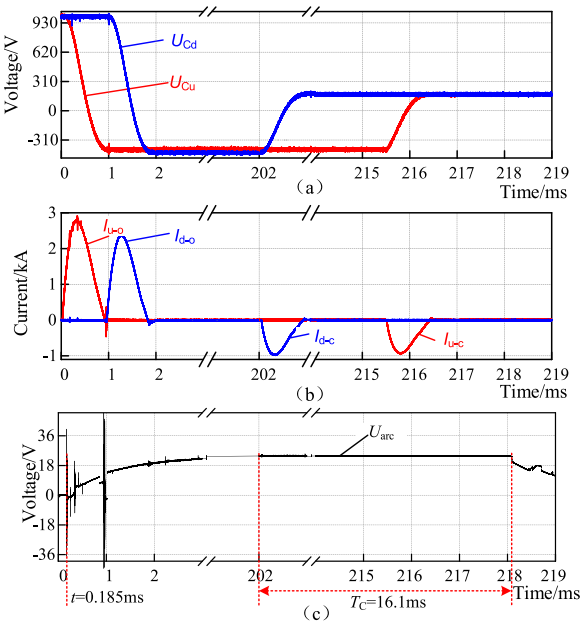

Fig. 7. Experimental results. (a) Voltage on capacitors (C_u, C_d). (b) Current though L_u and L_d. (c) Voltage across static contact and moving contact (U_{VS}).

B. Experimental Results

Sequential O-C operation test of the developed prototype is carried out, and the experimental results are illustrated in Figs. 7 and 8.

As shown in Fig. 8(a), when t = 0 ms, static contact and moving contact are compressed together, and U_{VS} is zero; U_{Cu} and U_{Cd} is 990 V.

As for the O-operation process, $T_{u\text{-}o}$, $T_{d\text{-}o}$ is triggered at t = 0 ms and t = 0.94 ms, respectively. As shown in Fig. 7, during the acceleration period of O-operation (0–0.94 ms), C_u discharges through L_u, generating pulse current ($I_{u\text{-}o}$) with amplitude of 2.8 kA. After the discharge, residual voltage of −420 V appears on C_u. During the deceleration period of metal disk for O-operation (0.94–2ms), C_d discharges through L_d, generating pulse current ($I_{d\text{-}o}$) with amplitude of 2.38 kA and residual voltage on C_d is −446 V, which is ∼45% of the initial voltage, meaning ∼20% of the initial energy returns back to C_u. Referring to Fig. 7(c), U_{VS} starts to increase at t = 0.185 ms, meaning contacts are separated at this moment, and this time delay is caused by the inertia of moving contact and the over-stroke (1 mm). Referring to Fig. 8(b), the metal disk moves to the O-position already at t = 2 ms, which validates the rapid O-operation of the prototype.

As shown in Fig. 8(d), moving contact is still in O-position at t = 202 ms. The time interval of 200 ms is reserved for the de-ionization of the fault point. Then, C-operation of the prototype is ignited with $T_{d\text{-}c}$ and $T_{u\text{-}c}$ triggered in sequence. During the acceleration period of C-operation (202–202.94 ms), C_d with voltage of −446 V discharges through L_d, generating pulse current ($I_{d\text{-}c}$) with amplitude of −0.97 kA. After the acceleration period, metal disk moves toward the C-position with almost constant velocity (202.94–215.6 ms). Then, with metal disk moving near to the C-position, C_u discharges through L_u to decelerate the metal disk.

TABLE II
PERFORMANCE COMPARISON

Items	Conventional operating method	Proposed operating method
Operating energy (J)	2038	1019
Number of capacitors	4	2
Number of thyristors	4	4
Size	4 × 2 × Φ85 mm × 175 mm	2 × 2 × Φ85 mm × 175 mm
Cost	1p.u.	0.55p.u.

Referring to Fig. 7(c), U_{VS} starts to decrease at 218.1ms, meaning C-operation is completed at this moment. Referring to Fig. 8(e), metal disk is in C-position at t = 218.1ms, meaning the C-operation of ultrafast VS takes 16.1 ms which is longer than the O-operation.

It should be noted, with the existence of friction force, parasitic resistance of coils, and the machining errors of coils and metal disk, there is an acceptable deviation between simulation results and experimental results. For example, the simulated and experimental time duration of pulse current is 1ms and 0.94ms, and this deviation is caused by the machining error of coils.

V. PERFORMANCE DISCUSSION

To prove superiority of the proposed operating method over the conventional operating method [10], the performance of ultrafast VS is evaluated in terms of operating-energy, volume, and cost.

From the design level, when using the conventional drive circuits of ultrafast VS, referring to Fig. 2(a), 4 capacitor banks and 4 thyristor modules are needed for sequential O-C operations. However, by using the proposed drive circuit in this article, only two capacitor banks and four thyristor modules are needed for sequential O-C operation. Therefore, the capacitor usage is reduced by 50%. According to the prototype in Section IV ($C_u = C_d = 1.04$ mF; $U_0 = U_{Cu} = U_{Cd} = 990$V), the precharge energy of each capacitor is $1/2 \times C \times U_0^2$, and using the proposed operating method can reduce the operating-energy from 2038 to 1019J, which are illustrated in Table II.

In terms of volume and cost, the proposed operating method is mainly focused on reducing the capacitor usage in Part-C of Fig. 1, and Part-A and Part-B remain unchanged. Only volume and cost of Part-C is discussed here. Referring to the prototype in Section IV, volume of thyristor modules is negligible in comparison to capacitors, and the price of thyristor is 10% of the capacitor. For the conventional drive circuit, the total cost is set as 1p.u. For the proposed drive circuit, the cost is 0.55 p.u. Therefore, the volume of the operating energy storage unit decreased 50%, and its cost including capacitors and thyristor modules decreased from 1 to 0.55 p.u.

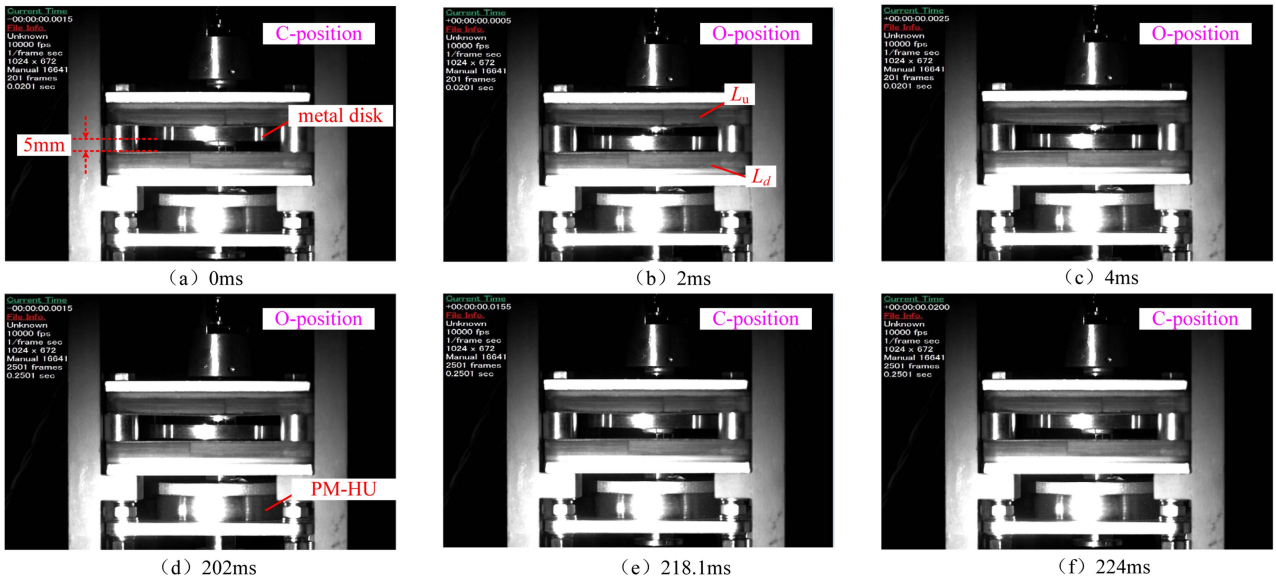

Fig. 8. Experimental results recorded by camera.

VI. Conclusion

Starting from the unique aspect of recycling residual energy in capacitors for sequential open-close operation, a high-efficient and miniaturized operating method for ultrafast VS in DCB is proposed in this article. Working principle of the proposed operating method is explained, and mathematical model in the form of differential equations is deduced and solved. Then, a prototype with rated parameters of 3.6 kV/2500 A/1 ms is established for experimental verification. The results show that by using the proposed operating method, the operating energy is reduced along with the improvement of operating-efficiency, and with capacitors usage reduced by 50%, both size and cost of the operating mechanism decrease significantly.

References

[1] W. Chen et al., "Development and prospect of direct-current circuit breaker in China," *High Voltage*, vol. 6, pp. 1–15, 2021.
[2] C. M. Franck, "HVDC circuit breakers: A review identifying future research needs," *IEEE Trans. Power Del.*, vol. 26, no. 2, pp. 998–1007, Apr. 2011, doi: 10.1109/TPWRD.2010.2095889.
[3] G. Tang et al., "Research and development of a full-bridge cascaded hybrid HVDC breaker for VSC-HVDC applications," *CIGRE*, vol. 2016, pp. 3–117, 2016.
[4] X. Zhang et al., "A state-of-the-art 500-kV hybrid circuit breaker for a dc grid: The world's largest capacity high-voltage dc circuit breaker," *IEEE Ind. Electron. Mag.*, vol. 14, no. 2, pp. 15–27, Jun. 2020.
[5] Y. Wu, Y. Wu, F. Yang, M. Rong, and Y. Hu, "Bidirectional current injection MVDC circuit breaker: Principle and analysis," *IEEE Trans. Emerg. Sel. Topics Power Electron.*, vol. 8, no. 2, pp. 1536–1546, Jun. 2020.
[6] J. He et al., "Review of DC circuit breaker technology development," *Southern Power Syst. Technol.*, vol. 9, no. 02, pp. 9–15, 2015.
[7] C. Xu, Z. Jin, M. Tousi, and L. Graber, "Critical damping in travel curves of piezoelectrically actuated fast mechanical switches for hybrid circuit breakers," *IEEE Trans. Power Del.*, vol. 37, no. 5, pp. 3873–3884, Oct. 2022.
[8] C. Xu et al., "Piezoelectrically actuated fast mechanical switch for MVDC protection," *IEEE Trans. Power Del.*, vol. 36, no. 5, pp. 2955–2964, Oct. 2021.
[9] D. Jovcic, "Fast commutation of DC current into a capacitor using moving contacts," *IEEE Trans. Power Del.*, vol. 35, no. 2, pp. 639–646, Apr. 2020.
[10] W. Wen et al., "Research on operating mechanism for ultra-fast 40.5-kV vacuum switches," *IEEE Trans. Power Del.*, vol. 30, no. 6, pp. 2553–2560, Dec. 2015.
[11] Y. Huang et al., "Research on an ultrafast driver for HVDC circuit breaker with electromagnetic repulsion mechanism," *High Voltage Eng.*, vol. 40, no. 10, pp. 3171–3178, 2014.
[12] B. Lequesne, T. Holp, S. C. Schmalz, R. Michael Slepian, and H. Wang, "Frequency-domain analysis and design of thomson-coil actuators," *IEEE Trans. Ind. Appl.*, vol. 59, no. 2, pp. 1765–1774, Mar./Apr. 2023.
[13] M.-S. Sim, S. S. H. Bukhari, and J.-S. Ro, "Analysis and design of a thomson coil actuator system for an HVDC circuit breaker," *IEEE Access*, vol. 10, pp. 58354–58359, 2022.
[14] W. Yang, F. Meng, X. Huang, and G. Zhai, "Soft-landing mechanism design driven by electromagnetic repulsion force with application to bypass switch," *IEEE Trans. Magn.*, vol. 59, no. 11, Nov. 2023, Art. no. 8500206.
[15] J. Jiang et al., "Research on the coordination of 40.5 kV fast vacuum switch driven by electromagnetic repulsion mechanism and oil damper," in *Proc. 5th Int. Conf. Electric Power Equip. - Switching Technol.*, 2019, pp. 652–657.
[16] T. Augustin, M. Parekh, J. Magnusson, M. Becerra, and H.-P. Nee, "Thomson-coil actuator system for enhanced active resonant DC circuit breakers," *IEEE J. Emerg. Sel. Topics Power Electron.*, vol. 10, no. 1, pp. 800–810, Feb. 2022, doi: 10.1109/JESTPE.2021.3083585.
[17] X. Pei, A. C. Smith, R. Shuttleworth, D. S. Vilchis-Rodriguez, and M. Barnes, "Fast operating moving coil actuator for a vacuum interrupter," *IEEE Trans. Energy Convers.*, vol. 32, no. 3, pp. 931–940, Sep. 2017.
[18] C. Peng, X. Song, A. Q. Huang, and I. Husain, "A medium-voltage hybrid DC circuit breaker—Part II: Ultrafast mechanical switch," *IEEE J. Emerg. Sel. Topics Power Electron.*, vol. 5, no. 1, pp. 289–296, Mar. 2017.
[19] W. Wen et al., "Novel reclosing strategy based on transient operating voltage in pseudobipolar DC system with mechanical DCCB," *IEEE Trans. Power Electron.*, vol. 36, no. 4, pp. 4125–4133, Apr. 2021.
[20] B. Li, J. He, Y. Li, and W. Wen, "A novel DCCB reclosing strategy for the flexible HVDC grid," *IEEE Trans. Power Del.*, vol. 35, no. 1, pp. 244–257, Feb. 2020.
[21] Vacuum interrupters, provided by ABB, 2023. [Online]. Available: https://search.abb.com/library/Download.aspx?DocumentID=DEABB%204068%20EN&LanguageCode=en&DocumentPartId=&Action=Launch
[22] The parameters for permanent NdFeB, 2023. [Online]. Available: http://www.zhongsheng-magnet.com/upload1/20170815/2017815143737.pdf
[23] W. Wen et al., "No-load dielectric recovery of the ultra-fast vacuum switch in hybrid dc circuit breaker," *IEEE Trans. Power Del.*, vol. 34, no. 3, pp. 840–847, Jun. 2019.